Volume 2
Number 8
August 2023
Pages 1067–1226

Energy Advances

rsc.li/energy-advances

ISSN 2753-1457

ROYAL SOCIETY OF CHEMISTRY

PAPER
Norazilawati Muhamad Sarih *et al.*
Poly(triazine-*co*-pyrrole)-based conjugated microporous polymers for carbon dioxide capture

Energy Advances

ROYAL SOCIETY OF CHEMISTRY

PAPER

View Article Online
View Journal | View Issue

Cite this: *Energy Adv.*, 2023, 2, 1127

Poly(triazine-*co*-pyrrole)-based conjugated microporous polymers for carbon dioxide capture†

Dushan Suranga Amaraseela, [a] Norazilawati Muhamad Sarih*[a] and Shehu Habibu [ab]

Received 8th December 2022,
Accepted 17th June 2023

DOI: 10.1039/d2ya00346e

rsc.li/energy-advances

Nowadays, conjugated microporous polymers (CMPs) are among the superior porous materials for carbon dioxide (CO_2) capture. The objective of this study was to accomplish oxidative copolymerization of 2,4,6-tris(5-bromothiophene-2-yl)-1,3,5-triazine and pyrrole in the presence of iron(III) chloride to produce a series of conjugated microporous polymers, TP-CMP-1, TP-CMP-2 and TP-CMP-3 for CO_2 capture applications. The monomers were employed at different molar ratios; the polymerization proceeded at room temperature, and subsequently, under solvothermal conditions to form a microporous network. The chemical structure of these TP-CMPs was ascertained using FTIR and solid ^{13}C NMR techniques. The TP-CMPs were further characterized for thermal and morphological studies and subsequently evaluated for CO_2 adsorption capacity. All the TP-CMPs showed exceptional thermal stability with decomposition temperatures ranging from 314 to 390 °C. Moreover, these TP-CMPs exhibited a Brunauer–Emmett–Teller (BET) surface area of up to 556 $m^2\ g^{-1}$, and CO_2 adsorption of up to 1.09 mmol g^{-1} at 298 K under 1 bar pressure. The high surface area facilitated great interactions with CO_2 molecules and enhanced carbon dioxide capture.

1. Introduction

Carbon dioxide (CO_2) is a major contributor to global warming and climate change, and its capture and storage have become a pressing environmental concern.[1,2] Current industrial applications of alkanolamine solvent systems to chemisorb CO_2 appear to exhibit several disadvantages of high-energy cost, solvent volatility, toxicity and equipment corrosion.[3–6]

Conjugated microporous polymers (CMPs) have emerged as promising materials for CO_2 capture due to their high surface area, porous structure, and tunable properties.[7–9] The significance of CMPs comes with the essential bond conjugation and amorphous morphology under microporous organic polymers (MOPs). Poly(arylene ethynylene)s were reported in 2007 as the first synthesized CMPs under palladium-catalyzed Sonogashira–Hagihara coupling by Cooper and his coworkers.[10] Although it was a recent addition to the MOP family, the first porous polymer synthesis was reported by Lloyd and Alfrey in the 1960s as a crosslinked poly(vinyl divinyl) network that was applied in solvent adsorption and later categorized under hypercrosslinked polymers (HCPs).[11,12] The family of MOPs extended with a few other classes such as covalent organic frameworks (COFs), polymers of intrinsic microporosity (PIMs) and porous aromatic frameworks (PAFs) are the main categories other than CMPs. The interest towards CMPs was drawn mainly due to their electronic and electroluminescent properties. A wide range of applications are so far reported using CMPs in the areas of gas storage,[13–16] catalysis,[17–20] light-emission,[21] light harvesting, and energy storage,[22,23] along with several other environmental (adsorption/separation)[24–27] and sensor[28,29] technologies.

Triazine-based porous polymers are yet another subclass of MOPs named as covalent triazine frameworks (CTFs), later copolymerized to build other classes like HCPs and CMPs contributing N-rich triazine to tailor the functionality and pore morphology. According to simulation studies and adsorption energetics, heteroatoms play a decisive role in carbon capture by forming dipolar–quadrupolar interactions with CO_2. The initial synthesis of covalent triazine-based frameworks was done by Kuhn *et al.* (2008) using di- and tri-nitrile substituted aromatic monomers cyclotrimerizing under ionothermal conditions over 400 °C with molten zinc(II) chloride.[30] Further studies led to the synthesis of CTFs at room temperature by

[a] *Department of Chemistry, Faculty of Science, Universiti Malaya, Kuala Lumpur 50603, Malaysia. E-mail: nmsarih@um.edu.my; Tel: +60379677173*
[b] *Department of Chemistry, Faculty of Science, Federal University Dutse, Dutse PMB 7651, Jigawa State, Nigeria*

† Electronic supplementary information (ESI) available. See DOI: https://doi.org/10.1039/d2ya00346e

Ren and coworkers,[31] using trifluoromethanesulfonic (triflic) acid as a strong Brønsted acid to catalyze nitrile trimerization producing > 1000 $m^2 g^{-1}$ surface area and 75.39 $cm^3 g^{-1}$ CO_2 uptake at 273 K/1 bar. The highest Brunauer–Emmett–Teller (BET) surface area (S_{BET}) of 995 $m^2 g^{-1}$ followed by the highest CO_2 adsorption capacity of 1.45 mmol g^{-1} was given by TNCMP-2, which was synthesized using 2,4,6-tris(4-bromophenyl)-1,3,5-triazine and tris(4-ethynylphenyl)amine. Kundu and Bhaumik[32] have studied the oxidative copolymerization of 2,4,6-tri(thiophene-2-yl)-1,3,5-triazine (TTPT) and thiophene building a copolymer network with higher amorphous nature. The resulting hypercrosslinked microporous copolymers (HCMs) had the highest surface area of 855 $m^2 g^{-1}$ shown by HCM-1 with TTPT:thiophene ratio 1 : 1, and the maximum CO_2 uptake of 2.6 mmol g^{-1} at 298 K/3 bar given by HCM-3 with TTPT:thiophene ratio 2 : 1.[32]

In this paper, we investigate the use of poly(triazine-*co*-pyrrole) based CMPs for CO_2 capture. We report the synthesis and characterization of these polymers and evaluate their performance for CO_2 adsorption. Our results show that these CMPs exhibit high CO_2 adsorption capacity and excellent selectivity over other gases, making them potential candidates for use in carbon capture applications. This study contributes to the development of sustainable and efficient materials for mitigating climate change.

2. Experimental

2.1 Chemicals

5-Bromothiophene-2-carboxaldehyde (95%), anhydrous iron(III) chloride (98%), trifluoromethanesulfonic acid (98%) and pyrrole (98%) were obtained from Sigma Aldrich. Tetrahydrofuran (99.8%), chloroform (99%), aqueous ammonia solution (25%), methanol (99.5%), *n*-hexane (96%) and acetone (98%) were purchased from Merck. Dichloromethane (99.5%) and sodium bicarbonate (99.7%) were obtained from Friendemann Schmidt. Resublimed iodine (99.8%) was purchased from R&M Chemicals while sodium thiosulfate pentahydrate (99%) was from Bendosen. All the solvents and reactants involved in synthesis such as 5-bromothiophene-2-carboxaldehyde (BTCHO) and pyrrole were dried before use. Furthermore, all the organic reactions were performed under a nitrogen (N_2) environment.

2.2 Synthesis of 2,4,6-tris(5-bromothiophene-2-yl)-1,3,5-triazine (triazine) monomer

The synthesis of the triazine was performed according to the method explained by Yasuda and his coworkers (Scheme S1 and S2) (Fig. S1) ESI.†[33]

2.3 Synthesis of triazine-pyrrole conjugated microporous polymers (TP-CMPs)

Triazine (1 mmol, 0.565 g) and pyrrole (1 mmol, 0.069 g) were dissolved in 40 ml of dried chloroform in a 250 ml round-bottom (RB) flask and stirred at room temperature under N_2. Meanwhile, anhydrous ferric chloride (16.14 mmol, 2.613 g) was dissolved in 40 ml of $CHCl_3$ using another RB flask and stirred at room temperature separately. After 1 h, the $FeCl_3$ mixture was slowly added to the monomer mixture and the reaction proceeded for 24 h at room temperature. Thereafter, the reaction mixture was added to a Teflon-lined autoclave and reacted under solvothermal conditions at 150 °C for 48 h (Scheme 1). A yellow-brown coloured gas was observed in the Teflon-lined autoclave suggesting the formation of HBr gas upon reaction between the triazine and pyrrole. The obtained solid copolymer was filtered and washed using methanol, acetone and dichloromethane followed by vacuum drying at 80 °C for 24 h. Further purification of TP-CMP was achieved using soxhlet extraction with methanol for 48 h and vacuum-dried for 24 h obtaining 0.6278 g of TP-CMP-1. Two other copolymers (TP-CMP-2 and TP-CMP-3) were synthesized varying the triazine:pyrrole ratios to 2 : 1 and 1 : 2 using the same amount of $FeCl_3$ under the same conditions as TP-CMP-1.

2.4 Characterization

The FTIR analysis was carried out using a PerkinElmer ATR-FTIR-spectrometer 400 (USA). Structure elucidation using $^1H/^{13}C$ nuclear magnetic resonance (NMR) was achieved using a Bruker Avance III HD 400 MHz (Switzerland) with 9.4 T magnetic field strength. Solid-NMR analysis was done using a Jeol JNM – ECX 500 (Japan) with 11.7 T magnetic field strength in zirconia rotors at 6 kHz/298 K. Microscopic analysis was carried out using the Hitachi SU8220 field emission scanning electron microscope (FESEM) system with 4–5 μm magnifications under 2 and 5 kV voltages. The Brunauer–Emmett–Teller

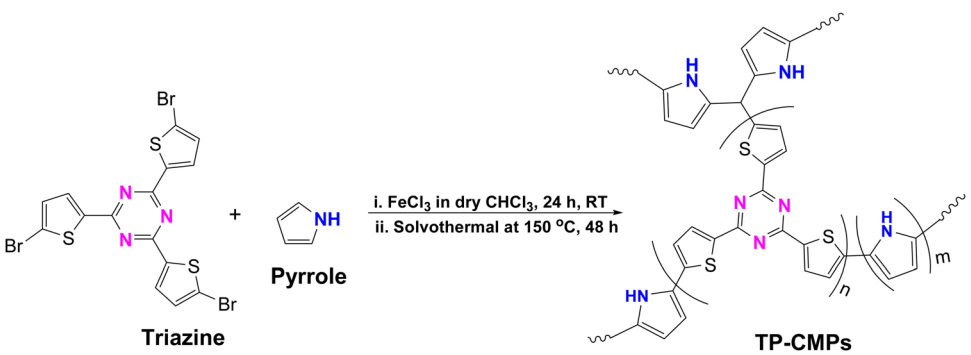

Scheme 1 Synthesis of the triazine-pyrrole conjugated microporous polymers (TP-CMPs).

(BET) isotherm analysis was achieved using BELSORP-mini II (USA) obtaining N_2 adsorption isotherms at 77 K. The copolymer samples were degassed under 6 mbar at 300 °C for 6 h before the N_2 isotherms were acquired. The adsorption capacity of CO_2 was evaluated using a Rubotherm gravimetric sorption analyzer with magnetic suspension balance (Germany) at 298 K and the pressure ranged from 0–30 bar. All copolymer samples were degassed at 120 °C for 2 h and buoyancy corrections were calibrated before taking the gravimetric measurements. The thermal stability of all TP-CMPs was analyzed by a PerkinElmer TGA4000 (USA) in a temperature range, of 30 °C to 850 °C at 10 °C min^{-1}. Powder X-ray diffraction (PXRD) was performed on all TP-CMPs using a Malvern PANalytical, Empyrean model (United Kingdom) between 5°–90° diffraction angles at 303 K temperature with the X-ray source CuKα (λ = 1.54 Å) of 4 kW power with 0.0472 deg s^{-1} angular velocity.

3. Results and discussion

The FTIR spectra of the synthesized copolymers are presented in Fig. 1. The broad peak around 1500 cm^{-1} can be attributed to either asymmetric C=C bond stretching of thiophene, C–C stretching of pyrrole or aromatic C–N stretching of triazine, where it may also appear as an overlapped peak of all three functionalities. However, the peak in the 1374–1369 cm^{-1} range also represents the aromatic C–N stretching of triazine. The stretching of pyrrole N–H is represented by the peak at around 3376 cm^{-1}, which has shifted from 3406 cm^{-1} of pristine poly(pyrrole) (Fig. S2, ESI†) and proved the success of the copolymerization (Fig. 1).[34] The stretching around 2978 cm^{-1} also indicates the presence of C–H in the thiophene rings of the copolymer. Furthermore, in-plane deformations of = C–H in pyrrole can be observed at 1255–1212 cm^{-1} in TP-CMP-1 and TP-CMP-3; meanwhile, TP-CMP-2 has shown 1191 cm^{-1} breathing vibrations of the pyrrole ring. The deformation vibration of C–H has again established that all the copolymers consist of pyrrole depicted by the peak around 787–754 cm^{-1}. The presence of triazine is further demonstrated by three C–S–C stretching peaks in all the TP-CMP spectra at around 1097–1054, 827–802 and 685–668 cm^{-1}.

Further characterization of the TP-CMP-2 structure was performed using ^{13}C CP/MAS NMR analysis as illustrated in Fig. 2. The region between 150–120 ppm can be identified as most of the thiophene and pyrrole ring C atoms represented by a broad and higher intensity peak.[34] The peak at 168 ppm represents triazine ring C atoms while the corresponding C_α atoms of thiophene and pyrrole groups overlap at 140 ppm. Around 134 ppm overlapping of the thiophene group C_β bonded with triazine causes peak broadening and the pyrrole C_β peak can be identified at 119 ppm in the spectrum.[32,35,36] Furthermore, overlapped peaks around 200 ppm are caused by the chemical shift anisotropy (CSA) effect by α and β carbons. In addition, Kundu and Bhaumik[32] have observed a peak around 50 ppm in their triazine-thiophene copolymer, assigned as an alkyl C atom bonded to three polymer chains either from thiophene or pyrrole ends. Hence, the peak at 50 ppm is identified as a tertiary C.

The thermal stability of TP-CMPs was analyzed using TGA from ~ 30–800 °C (Fig. S3, ESI†). The thermal analysis became necessary due to the possibility of exposing the material to high application temperature. From the TGA result of the prepared TP-CMPs, weight loss of about 2% has been observed below 100 °C in the case of TP-CMP-1, and 3.5% in TP-CMP-3 while TP-CMP-2 showed no such weight loss. The said weight loss may be attributed to the evaporation of adsorbed moisture onto the polymer, which is absent in the case of TP-CMP-2, which did not adsorb the moisture significantly.[37,38] Further weight loss was observed in all the CMPs as they degraded under an oxygenated environment. Each copolymer has a different onset of degradation temperature. TP-CMP-1 started degrading at around 345 °C. However, there is another weight loss around 220 °C which has not been observed in the other two TP-CMPs. This additional weight loss could be due to the decomposition of the poly(pyrrole) chain bonded with another substance.[39] The onset of thermal degradation of TP-CMP-2 is observed around 390 °C while the TP-CMP-3 exhibited the least onset degradation temperature at around 314 °C. The slight variation in the thermal stability of these polymers is possibly linked to differences in the monomer ratio of Triazine:pyrrole. Generally, all the polymer networks demonstrated almost the same

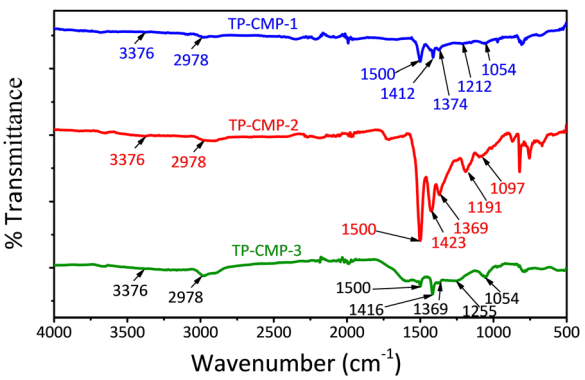

Fig. 1 FTIR spectra of TP-CMP-1, TP-CMP-2 and TP-CMP-3.

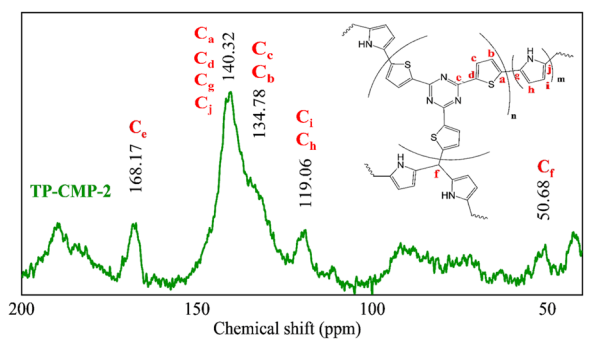

Fig. 2 Plausible structure of TP-CMPs and ^{13}C CP/MAS NMR spectrum of TP-CMP-2, 200–20 ppm.

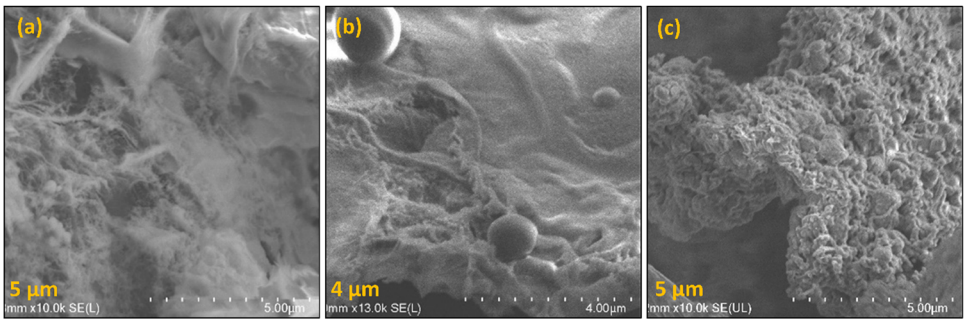

Fig. 3 FESEM images of (a) TP-CMP-1, (b) TP-CMP-2 and (c) TP-CMP-3.

thermal properties, since they have the same structure and functional groups.

As a preliminary analysis, FESEM was conducted, and Fig. 3 illustrates the results. The maximum magnification of 4–5 µm enables one to visualize the bulky nature of TP-CMPs suggesting the microporous nature of these polymers.

PXRD is one of the techniques used to assess the crystalline nature of materials. The PXRD spectra of the synthesized copolymers are presented in Fig. S4 (ESI†). TP-CMP-2 and TP-CMP-3 consist of sharp peaks to a certain extent, while TP-CMP-1 hardly shows any sharp peaks. Even though some sharp peaks with lower intensity values are found in TP-CMP-2 and TP-CMP-3, suggesting minimum crystalline content, it is clear that all three copolymers are amorphous in nature. There are a few crystalline-like peaks at lower 2θ angles below 10° suggesting in-plane reflections of the ideal poly(triazine) structure fraction of the copolymers.[40] Nevertheless, when the triazine is copolymerized with another monomer, especially functioning as a linker, it may lead to an amorphous character in the copolymer.

BET isotherm analysis is one of the most convenient techniques to perform the characterization of porous materials. The three most important characteristics of microporous materials like surface area, particle size distribution (PSD) and pore volume, which can be determined using N_2 adsorption-desorption isotherms at 77 K, are presented in Fig. 4(a).[41] The adsorption isotherms were plotted with adsorbed N_2 gas mols against the equilibrium pressure under 101.33 kPa (1.01 bar) total pressure. Non-local density functional theory (NLDFT) was adopted in calculating the PSD deriving average pore diameters of each TP-CMP.

Among the three polymers prepared, TP-CMP-2 exhibited the highest S_{BET} value of 556.58 $m^2\ g^{-1}$. Moreover, TP-CMP-2 possessed the highest pore volume of 0.2897 $cm^3\ g^{-1}$ as well as the least average pore diameter of 2.0819 nm. On the other hand, TP-CMP-3 had the lowest S_{BET} of 17.896 $m^2\ g^{-1}$ and the highest average pore diameter of 16.256 nm, as well as the least total pore volume of 0.0727 $cm^3\ g^{-1}$. TP-CMP-1 showed the medium values of S_{BET}, 473.77 $m^2\ g^{-1}$ along with 2.2607 nm average pore diameter as well as 0.2679 $cm^3\ g^{-1}$ total pore volume. As illustrated in Fig. 4(a), the adsorption measurements are between 0–0.99 equilibrium pressure (p/p_0) range of N_2 gas. In this adsorption isotherm, both TP-CMP-1 and 2 show adsorption range between 1–9 mmol g^{-1} under the above mentioned conditions. However, for TP-CMP-3 its N_2 adsorption capacity ranged between 0 and 3 mmol g^{-1} deriving the lowest S_{BET} in the equilibrium pressure range below 0.01. A rapid increase in N_2 adsorption followed by very slower gas uptake increment in the middle region and another higher gas adsorption above 0.9 equilibrium pressure was observed. This

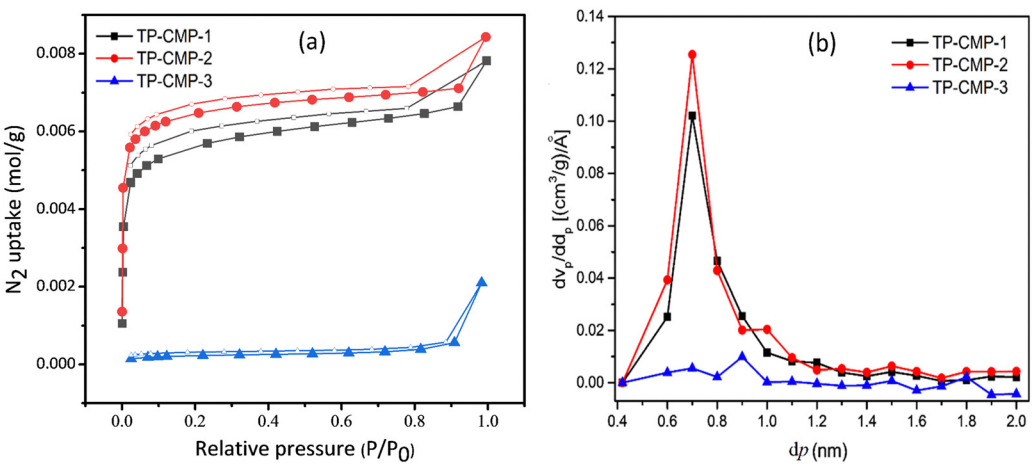

Fig. 4 (a) BET adsorption–desorption isotherms (coloured symbols – adsorption, empty symbols – desorption). (b) PSD plot of the TP-CMPs.

behaviour suggests that the isotherms can be approximately correlated to type IV indicating higher microporosity including a lower mesoporous nature.[42] Nevertheless, the TP-CMP-3 isotherm has a slightly deviated nature compared to TP-CMP-1 and TP-CMP-2 isotherms. The TP-CMP-3 isotherm can also be regarded as a microporous material. All these isotherms have shown a broad p/p_0 hysteresis loop between adsorption and desorption processes suggesting the existence of a metastable state.[43] The thiophene groups tend to possess lower rigidity resulting in a polymer matrix with a swelling efficiency under pressure difference, and this may be the cause of the hysteresis loop.[43] In addition, the phenomenon of capillary condensation is also indicated by this hysteresis loop.

Determination of PSD has further proceeded using micropore (MP) plots derived from the *t*-plot method presented in Fig. 4(b). Microporous and mesoporous cumulative volumes can be determined depending on each pore size illustrated in the *t*-plot where the MP-plot is plotted as a pore volume derivative of micropore size (dV_p/dd_p) against the micropore size (d_p).[44] Fig. 4(b) presents the most contribution to micropore volumes of TP-CMP-1, TP-CMP-2 and TP-CMP-3 given by the pores with diameters of 0.7, 0.7 and 0.9 nm, respectively. As illustrated in MP-plots, TP-CMP-1 and TP-CMP-2 have shown a greater contribution of micropores below 2 nm diameter to the pore volume. The peaks in the MP-plots are presented as pore diameter concentrated around 0.7 nm with $\sim$ 1.0 and 1.25 ($cm^3\ g^{-1}$) $Å^{-1}$ dV_p/dd_p values on TP-CMP-1 and TP-CMP-2. In contrast, TP-CMP-3 has shown a lower contribution of micropores to the pore volume where only a maximum of around 0.06 ($cm^3\ g^{-1}$) $Å^{-1}$ is observed compared to TP-CMP-1 and TP-CMP-2. Furthermore, the MP-plot of TP-CMP-3 shows higher peaks above 2 nm in the mesoporous region.

The high surface areas, low pore size distributions and presence of N and S atoms on the surfaces of these copolymers have motivated us to examine the carbon dioxide uptake capacity. Carbon dioxide adsorption isotherms of the microporous copolymers, TPCMP-1, TP-CMP-2, and TP-CMP-3, at 298 K and 0–30 bar are depicted in Fig. 5. The adsorption capacity was measured using a gravimetric sorption analyzer under isothermal conditions. The highest value of CO_2 uptake of 48.00 mg g^{-1} (1.09 mmol g^{-1}) is exhibited by TP-CMP-2 at 1 bar pressure. On the other hand, TP-CMP-3 showed the lowest CO_2 uptake of 31.29 mg g^{-1} (0.71 mmol g^{-1}) at the same pressure and temperature. While TP-CMP-1 had a much closer value of CO_2 adsorption capacity to TP-CMP-2, around 46.32 mg g^{-1} (1.05 mmol g^{-1}) at 1 bar and 298 K. However, at 30 bar the difference between adsorption values has further deviated resulting in 142.43 mg g^{-1} and 150.64 mg g^{-1} for TP-CMP-1 and TP-CMP-2, respectively. While TP-CMP-3 has exhibited a maximum adsorption of 66.20 mg g^{-1} at the same pressure. Therefore, the optimum composition of TP-CMPs for the highest surface area followed by the highest CO_2 adsorption capacity are held by the composition of triazine:pyrrole 2 : 1 as represented by TP-CMP-2.

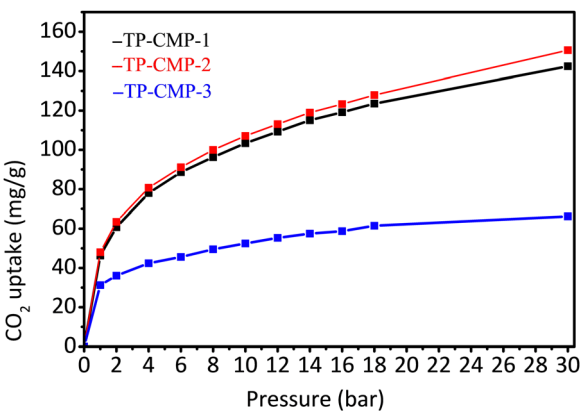

Fig. 5 CO_2 adsorption isotherms at 298 K from 0–30 bar of TP-CMPs.

Based on the isotherm behavior, within the initial region between 0–3 bar, there are greater gradients in gas uptake, which was eventually reduced at higher pressure values. TP-CMP-1 and TP-CMP-2 did not show a saturation from CO_2 even at the highest experimental pressure of 30 bar, while TP-CMP-3 has shown approximately a plateau behavior. According to Liu and coworkers (2012), the adsorption at lower pressure would be dominated by interactions of the adsorbent, derived from chemical functionalities. Moreover, at higher pressures, the gas adsorption would be limited by the surface area of the adsorbent, which allows for interaction with the adsorbate.[45] The chemical composition of TP-CMPs consists of heteroatoms N and S at higher ratio compared with C under different functional groups. Hence, they are capable of interacting with CO_2 using dipole–quadrupole interactions, which mostly contributed to low pressure adsorption. However, the adsorption capacity correlates to the S_{BET} values where the highest surface area TP-CMP-2 has the highest CO_2 uptake. Adsorption capacity values against the BET isotherm data are presented in Table 1.

In addition, the adsorption isotherms are more distinguished when the pressure of the CO_2 has increased as presented in Fig. 5, providing evidence for the assumption that higher adsorbate pressure gas uptake is governed by the adsorbent surface area.

Remarkably, the CO_2 uptake capacity of our tested CMPs is among the highest reported for N containing CMPs. Moreover, they represented a significant CO_2 adsorption capacity relative to other porous substances.[46–50] The observed values of CO_2 adsorption capacity have confirmed our submission that the strong interactions that exist between our CMPs and CO_2 molecules are similar to the behavior of other CMPs reported (Table 2).

Table 1 Physical characteristics with CO_2 uptake of TP-CMPs

TP-CMP	Triazine: Pyrrole	S_{BET} ($m^2\ g^{-1}$)	Average pore diameter (nm)	Total pore volume ($cm^3\ g^{-1}$)	CO_2 uptake (mmol g^{-1}) at 298 K/1 bar
1	1 : 1	473.77	2.2607	0.2678	1.05
2	2 : 1	556.58	2.0819	0.2897	1.09
3	1 : 2	17.896	16.256	0.0727	0.71

Table 2 CO_2 adsorption capacity values of TP-CMPs prepared in the present study compared with those of other reported CMPs

CMP	S_{BET} (m^2 g^{-1})	CO_2 uptake (mmol g^{-1}) at 298 K	Pressure (bar)	Ref.
TP-CMP-1	473.77	1.05	1	Present study
TP-CMP-2	556.58	1.09	1	Present study
TP-CMP-3	17.896	0.71	1	Present study
HMC-1	855	2.4	3	32
HMC-2	425	1.9	3	32
HMC-3	566	2.6	3	32
ETM-1	368	2.11	1	50
TFM-1	738	0.86	1	48
Azo-Cz-CMP	315	0.8	1	46
PC	339	3.2	1	51
HPANI-5	461	0.59	1	4
TPI-1	809	1.25	1	52
TPI-3	40	0.43	1	52

4. Conclusion

A novel strategy for the synthesis of TP-CMPs with higher N and S composition microporous triazine-based polypyrrole copolymers having good thermal stability and high BET surface area has been reported in the current study. FTIR and solid-state NMR spectroscopic techniques were used to ascertain the chemical structure of these polymers. The highest S_{BET} value of 556 m^2 g^{-1} was given by TP-CMP-2 having the composition of triazine:pyrrole, 2 : 1. Owing to its reasonable surface area, TP-CMP-2 exhibited good CO_2 uptake of 1.09 mmol g^{-1} at 298 K/1 bar. Based on their CO_2 uptake ability, as well as their good physicochemical stability, these materials can be considered among the promising candidates for gas separation and storage applications. Hence, they can be potentially exploited in carbon dioxide removal techniques towards the re-establishment of a cleaner environment.

Author contributions

Conceptualization: Norazilawati Muhamad Sarih; methodology: Norazilawati Muhamad Sarih, Dushan Suranga Amaraseela; formal analysis and investigation: Norazilawati Muhamad Sarih, Dushan Suranga Amaraseela and Shehu Habibu; writing – original draft preparation: Dushan Suranga Amaraseela; writing – review and editing: Norazilawati Muhamad Sarih, and Shehu Habibu; funding acquisition: Norazilawati Muhamad Sarih; resources: Norazilawati Muhamad Sarih; supervision: Norazilawati Muhamad Sarih.

Conflicts of interest

The authors declare that they have no known competing financial interests or personal relationships that could have appeared to influence the work reported in this paper.

Acknowledgements

This work was supported by the Fundamental Research Grant, FRG (FG042-17AFR) and the Impact-Oriented Interdisciplinary Research Grant, IIRG (IIRG006A-19IISS) of Universiti Malaya, Malaysia. We are grateful to the Department of Chemistry, Faculty of Science, Universiti Malaya, Malaysia for facilitating this study. The financial assistance provided by both FRG and IIRG is highly appreciated by the authors.

References

1 M. Bui, C. S. Adjiman, A. Bardow, E. J. Anthony, A. Boston, S. Brown, P. S. Fennell, S. Fuss, A. Galindo, L. A. Hackett, J. P. Hallett, H. J. Herzog, G. Jackson, J. Kemper, S. Krevor, G. C. Maitland, M. Matuszewski, I. S. Metcalfe, C. Petit, G. Puxty, J. Reimer, D. M. Reiner, E. S. Rubin, S. A. Scott, N. Shah, B. Smit, J. P. M. Trusler, P. Webley, J. Wilcox and N. Mac Dowell, *Energy Environ. Sci.*, 2018, **11**, 1062–1176.
2 W. Gao, S. Liang, R. Wang, Q. Jiang, Y. Zhang, Q. Zheng, B. Xie, C. Y. Toe, X. Zhu, J. Wang, L. Huang, Y. Gao, Z. Wang, C. Jo, Q. Wang, L. Wang, Y. Liu, B. Louis, J. Scott, A.-C. Roger, R. Amal, H. He and S.-E. Park, *Chem. Soc. Rev.*, 2020, **49**, 8584–8686.
3 X. Jiang, Y. Kong, H. Zou, Z. Zhao, Y. Zhong and X. Shen, *J. Porous Mater.*, 2021, **28**, 93–97.
4 W. Tang, Y. Wu, A. Xu, T. Gao, Y. Wei and G. Zhou, *J. Porous Mater.*, 2019, **26**, 1495–1505.
5 B. Szczęśniak, Ł. Osuchowski, J. Choma and M. Jaroniec, *J. Porous Mater.*, 2018, **25**, 621–627.
6 Z. Liu, Y. Zhu, Z. Du, W. Xing, S. Komarneni and Z. Yan, *J. Porous Mater.*, 2015, **22**, 1663–1672.
7 M. Sai Bhargava Reddy, D. Ponnamma, K. K. Sadasivuni, B. Kumar and A. M. Abdullah, *RSC Adv.*, 2021, **11**, 12658–12681.
8 D. Taylor, S. J. Dalgarno, Z. Xu and F. Vilela, *Chem. Soc. Rev.*, 2020, **49**, 3981–4042.
9 Y. Zhang, F. Tian, X. Guo, M. Bai, T. Tang, X. Di, W. Wang, Z. Liu and X. Shao, *Sustainable Energy Fuels*, 2023, **7**, 2063–2073.
10 J. X. Jiang, F. Su, A. Trewin, C. D. Wood, N. L. Campbell, H. Niu, C. Dickinson, A. Y. Ganin, M. J. Rosseinsky, Y. Z. Khimyak and A. I. Cooper, *Angew. Chem., Int. Ed.*, 2007, **46**, 8574–8578.
11 W. G. Lloyd and T. Alfrey Jr, *J. Polym. Sci.*, 1962, **62**, 301–316.
12 G. Kupgan, L. J. Abbott, K. E. Hart and C. M. Colina, *Chem. Rev.*, 2018, **118**, 5488–5538.
13 C. Zhang, X. Yang, Y. Zhao, X. Wang, M. Yu and J.-X. Jiang, *Polymer*, 2015, **61**, 36–41.
14 D. Chang, M. Yu, C. Zhang, Y. Zhao, R. Kong, F. Xie and J.-X. Jiang, *Microporous Mesoporous Mater.*, 2016, **228**, 231–236.
15 R. Dawson, A. I. Cooper and D. J. Adams, *Polym. Int.*, 2013, **62**, 345–352.
16 N. Manoranjan, J. Kim, S. I. Woo and D. H. Won, *J. CO2 Util.*, 2016, **16**, 486–491.

17 S. Ghasimi, S. A. Bretschneider, W. Huang, K. Landfester and K. A. I. Zhang, *Adv. Sci.*, 2017, **4**, 1700101.
18 Y. Xu, C. Zhang, P. Mu, N. Mao, X. Wang, Q. He, F. Wang and J.-X. Jiang, *Sci. China: Chem.*, 2017, **60**, 1075–1083.
19 Y. B. Zhou and Z. P. Zhan, *Chem. – Asian J.*, 2018, **13**, 9–19.
20 C. Ayed, W. Huang, R. Li, L. C. daSilva, D. Wang, O. Suraeva, W. Najjar and K. A. I. Zhang, *Part. Part. Syst. Charact.*, 2018, **35**, 1700234.
21 B. D. To, H. C. Chen, D. D. Nguyen, W. Y. Yeh, J.-R. Ho, H.-C. Kan and C. C. Hsu, *Org. Electron.*, 2018, **59**, 164–170.
22 C. Zhang, Y. He, P. Mu, X. Wang, Q. He, Y. Chen, J. Zeng, F. Wang, Y. Xu and J. X. Jiang, *Adv. Funct. Mater.*, 2018, **28**, 1705432.
23 Y. Kou, Y. Xu, Z. Guo and D. Jiang, *Angew. Chem., Int. Ed.*, 2011, **50**, 8753–8757.
24 Y. Liao, J. Weber, B. M. Mills, Z. Ren and C. F. J. Faul, *Macromolecules*, 2016, **49**, 6322–6333.
25 L. Xiang, Y. Zhu, S. Gu, D. Chen, X. Fu, Y. Zhang, G. Yu, C. Pan and Y. Hu, *Macromol. Rapid Commun.*, 2015, **36**, 1566–1571.
26 D. Xu, W. D. Wu, H.-J. Qi, R.-X. Yang and W.-Q. Deng, *Chemosphere*, 2018, **196**, 174–181.
27 T. Geng, W. Zhang, Z. Zhu and X. Kai, *Microporous Mesoporous Mater.*, 2019, **273**, 163–170.
28 W. E. Lee, Y. J. Jin, L. S. Park and G. Kwak, *Adv. Mater.*, 2012, **24**, 5604–5609.
29 V. M. Suresh and U. Scherf, *Macromol. Chem. Phys.*, 2018, **219**, 11.
30 P. Kuhn, M. Antonietti and A. Thomas, *Angew. Chem., Int. Ed.*, 2008, **47**, 3450–3453.
31 S. Ren, M. J. Bojdys, R. Dawson, A. Laybourn, Y. Z. Khimyak, D. J. Adams and A. I. Cooper, *Adv. Mater.*, 2012, **24**, 2357–2361.
32 S. K. Kundu and A. Bhaumik, *ACS Sustainable Chem. Eng.*, 2016, **4**, 3697–3703.
33 T. Yasuda, T. Shimizu, F. Liu, G. Ungar and T. Kato, *J. Am. Chem. Soc.*, 2011, **133**, 13437–13444.
34 A. Nan, I. Craciunescu, R. Turcu, D. Reichert and J. Liebscher, *J. Optoelectron. Adv. Mater.*, 2008, **10**, 2265.
35 S. Ren, R. Dawson, A. Laybourn, J.-X. Jiang, Y. Khimyak, D. J. Adams and A. I. Cooper, *Polym. Chem.*, 2012, **3**, 928–934.
36 Y. Zhang, A. Sigen, Y. Zou, X. Luo, Z. Li, H. Xia, X. Liu and Y. Mu, *J. Mater. Chem. A*, 2014, **2**, 13422–13430.
37 B. A. Akinyemi and T. E. Omoniyi, *J. Indian Acad. Wood Sci.*, 2018, **15**, 45–51.
38 S. Vyazovkin, A. K. Burnham, J. M. Criado, L. A. Pérez-Maqueda, C. Popescu and N. Sbirrazzuoli, *Thermochim. Acta*, 2011, **520**, 1–19.
39 M. T. Ramesan, *J. Appl. Polym. Sci.*, 2013, **128**, 1540–1546.
40 P. Katekomol, J. Roeser, M. Bojdys, J. Weber and A. Thomas, *Chem. Mater.*, 2013, **25**, 1542–1548.
41 M. S. Mel'gunov and A. B. Ayupov, *Microporous Mesoporous Mater.*, 2017, **243**, 147–153.
42 K. S. Sing, *Pure Appl. Chem.*, 1985, **57**, 603–619.
43 S. Qiao, Z. Du and R. Yang, *J. Mater. Chem. A*, 2014, **2**, 1877–1885.
44 A. Galarneau, F. Villemot, J. Rodriguez, F. Fajula and B. Coasne, *Langmuir*, 2014, **30**, 13266–13274.
45 J. Liu, P. K. Thallapally, B. P. McGrail, D. R. Brown and J. Liu, *Chem. Soc. Rev.*, 2012, **41**, 2308–2322.
46 A. F. Saber, K.-Y. Chen, A. F. M. EL-Mahdy and S.-W. Kuo, *J. Polym. Res.*, 2021, **28**, 1–12.
47 R. L. Thankamony, X. Li, S. K. Das, M. M. Ostwal and Z. Lai, *J. Membr. Sci.*, 2019, **591**, 117348.
48 X. Zhu, C. Tian, S. M. Mahurin, S.-H. Chai, C. Wang, S. Brown, G. M. Veith, H. Luo, H. Liu and S. Dai, *J. Am. Chem. Soc.*, 2012, **134**, 10478–10484.
49 S. K. Kundu and A. Bhaumik, *ACS Sustainable Chem. Eng.*, 2016, **4**, 3697–3703.
50 S. Pourebrahimi and M. Pirooz, *Chem. Eng. J. Adv.*, 2022, **11**, 100315.
51 Z. Li, W. Wang, Y. Xu, Y. Zhu and X. Guo, *J. CO2 Util.*, 2021, **49**, 101550.
52 M. R. Liebl and J. Senker, *Chem. Mater.*, 2013, **25**, 970–980.